

Smeared Crack Models for Reinforced Concrete Beams by Finite Element Method

Modelos de Fissuração Distribuída em Vigas de Concreto Armado pelo Método dos Elementos Finitos



R.C.G. MENIN ^a
renatomenin@gmail.com

L.M. TRAUTWEIN ^b
leandromt@gmail.com

T.N. BITTENCOURT ^c
tbitten@gmail.com

Abstract

The main goal of the present work is to present a comparison between two different strategies for the computational simulation of reinforced concrete structures, both using smeared crack models to represent the behavior of the materials. As a first approach, a multidirectional smeared crack model available in DIANA has been adopted along with different softening rules for the cracked materials (brittle, linear, non-linear of Moelands-Reinhardt and Hordijk). Additionally, the Disturbed Stress Field Model – DSFM has also been adopted to model cracked concrete as an orthotropic material with smeared rotating cracks. The finite element codes DIANA and VecTor2 have been used to evaluate the performance of the different smeared crack models to predict the behavior of reinforced concrete beams subjected primarily to flexure.

Keywords: *smeared crack, reinforced concrete, finite element method.*

Resumo

O objetivo principal do trabalho é apresentar uma comparação entre distintas estratégias de simulação computacional de estruturas de concreto armado utilizando modelos de fissuração distribuída. Em uma primeira abordagem, foi adotado o modelo multidirecional de fissuração distribuída do programa DIANA empregando-se diferentes regras de amolecimento para o material fissurado (frágil, linear e não-lineares de Moelands-Reinhardt e de Hordijk). Posteriormente, foi utilizada a formulação DSFM – Disturbed Stress Field Model, modelando o concreto fissurado como um material ortotrópico com fissuras distribuídas do tipo rotacionais. Os programas DIANA e VecTor2 foram utilizados como ferramentas para avaliar a eficácia dos diferentes modelos no estudo de vigas de concreto armado submetidas a esforços de flexão.

Palavras-chave: *fissuração distribuída, concreto armado, método dos elementos finitos.*

^a Grupo de Modelagem de Estruturas de Concreto / GMEC, Departamento de Engenharia de Estruturas e Geotécnica, Escola Politécnica da Universidade de São Paulo / EPUSP, renatomenin@gmail.com, Av. Prof. Almeida Prado tv.2, n.83
Cidade Universitária CEP 05508-900, São Paulo, Brasil;

^b Grupo de Modelagem de Estruturas de Concreto / GMEC, Departamento de Engenharia de Estruturas e Geotécnica, Escola Politécnica da Universidade de São Paulo / EPUSP, leandromt@gmail.com, Av. Prof. Almeida Prado tv.2, n.83
Cidade Universitária CEP 05508-900, São Paulo, Brasil;

^c Grupo de Modelagem de Estruturas de Concreto / GMEC, Departamento de Engenharia de Estruturas e Geotécnica, Escola Politécnica da Universidade de São Paulo / EPUSP, tbitten@gmail.com, Av. Prof. Almeida Prado tv.2, n.83,
Cidade Universitária CEP 05508-900, São Paulo, Brasil.

1. Introduction

The reinforced concrete became one of the most important structural materials in the last century, being widely used in different areas of civil engineering. Due its low resistance to tensile stresses, the concrete structures suffer cracks even when they are subjected to low levels of load, which causes a reduction on their stiffness and modify the internal stress distribution, and as a result the structure starts to present a non-linear behavior.

The crack modeling is a quite complex and intriguing topic for being associated to the discontinuity study in the displacement field. In the numerical simulation of reinforced concrete structures by Finite Element Method, three different tendencies have been developed to represent the cracks: discrete, smeared and incorporated.

The discrete crack models are based on the idea of always working with the portion of the solid which remains continuous and without any damages, so that during the formation or progression of an existing crack, its sides incorporate to the outline of the solid. The cracks are modeled as displacement discontinuities among the finite elements and they must develop across their outlines, what ends up generating a restriction in its propagation direction. The application of these models is limited to the study of the problems involving the progression of few cracks, what hinders its use in most of the reinforced concrete structures.

In the smeared crack models, the cracked material is treated as continuous, and the discontinuity of the displacement field caused by the crack is spread across the element by changing the constitutive equation. Despite the successful study of most of the reinforced concrete structures, among the deficiencies of these models, it can be pointed out the difficulty in studying the localized cracking situations, as well as the sensitivity problems concerning the finite element mesh.

Later on, the incorporated crack models appeared which gather the favorable aspects of the previous two tendencies: there is no need of a mesh redefinition (deficiency observed in the discrete model) and the results obtained are independent from the finite element mesh (deficiency of the smeared model). The models are based on the concept of discontinuities incorporated in standard finite elements.

2. Smeared crack models

Since it has begun to be used in reinforced concrete structures, the Finite Element Method has shown more advantages by representing the cracks through changes of the constitutive equations (smeared models) instead of changes on the finite element mesh (discrete models). The first analyses were based on the idea of fragile failure, that is, to make the material stiffness null in the direction of the maximum tensile stress when it exceeded the tensile strength.

Later on, it was observed that better results in the post-peak phase could be achieved by adopting a gradual reduction in the stress. In order to represent this behavior, the stress-strain diagram started to be defined by experimental values and, thus, several models were proposed (Cedolin e Dei Poli [1], Bazant and Gambarova [2], Gupta and Maestrini [3], and Vecchio [4]).

Though successfully used to represent the behavior of the reinforced concrete structures which presented a crack pattern well distributed, when used to simulate the behavior of structures in which a crack is predominant (plain concrete or deep beams), these

models presented some deficiencies. One of the deficiencies is the sensitivity regarding the mesh, caused by the non-consideration of concepts associated to Fracture Mechanics. So, it was necessary to apply the Fracture Mechanics concepts directly over the concrete structures analysis, creating a series of new models (Bazant and Cedolin [5], Bazant and Oh [6], Feestra and de Borst [7]).

Rots and Blaauwendraad [8] presented a comparative study between the discrete and smeared crack models. This study introduced the idea of dividing the smeared crack models into fixed and rotating. In the fixed model, the crack orientation is kept constant during the whole computational process, while in the rotating model the crack orientation may change, following the main directions. There is also an intermediary option which is the concept of multidirectional fixed smeared crack.

There are also the models based on the plasticity theory, which are able to represent well the pre-peak and post-peak phases, consisting of a constitutive model and a failure criterion. In this line it can be pointed out the models by Ottosen [9] and Pramono and Willam [10].

3. Smeared crack models in DIANA

DIANA code – version 9.1 was used to evaluate the performance of different smeared crack models. DIANA is a finite element software based on the displacement method for non-linear analysis of concrete structures, which has been developed since 1972 by Delft University of Technology in Netherlands.

The smeared crack models are defined through the combination of three factors: a failure criterion (constant or linear), the cut transfer through the crack (total, constant or variable) and the material softening behavior (brittle, linear, multilinear or non-linear). In order to enable the combination of the crack model with a plastic behavior of the material, the total strain, ϵ , is decomposed in two parts, one is the elastic strain, ϵ^e , and the other is the crack strain, ϵ^{cr} . In the definition of the constitutive model, a criterion for the beginning of a new crack and its stress-strain relationship must still be established.

For the beginning of a new crack, two pre-requirements are necessary: the principal stress must exceed a limit stress; and, in case there is a previous crack, the angle between the existing crack and the principal tensile stress must exceed the initial crack angle. Regarding the constitutive model, the stress-strain relationship in the normal direction of the crack may be expressed by:

$$\sigma^{cr}(\epsilon^{cr}) = f_t y \left(\frac{\epsilon^{cr}}{\epsilon_{ult}} \right) \quad (1)$$

where, f_t is the concrete tensile strength and the variable y is the function that represents the material softening diagram. The ultimate strain ϵ_{ult} is assumed to be constant, and it may be obtained from the concrete tensile strength f_t , the fracture energy G_f , and the element area (represented by its equivalent length h):

$$\epsilon_{ult} = \frac{1}{\alpha} \left(\frac{G_f}{hf_t} \right) \quad (2)$$

where:

$$\alpha = \int_{x=0}^{x=\infty} y(x)dx \quad e \quad x = \frac{\epsilon^{cr}}{\epsilon_{ult}} \quad (3)$$

The fracture energy G_f may be calculated in two ways: the first one based on the model code CEB-FIP [11] and the second based on the laws of the softening and hardening branches of concrete. Another possibility is to use the hardening-softening laws with rheological models originated from the plasticity theory. Among the smeared crack models available in DIANA, it may be pointed out: fixed, multidirectional and rotating models. In the present work just the multidirectional smeared crack models were used.

3.1 Multidirectional smeared crack models

The multidirectional smeared crack models are known for presenting an intermediary behavior between the fixed and rotating models. These models allow the propagation of several cracks at the same point and according to the definition of the parameter called "threshold angle", a fixed or rotating model may be obtained. This parameter represents the angle between an existing crack and another one formed at the same point and its standard value is 60°. If this parameter is changed to 90°, a fixed model is obtained and if changed to 0° a rotating model is obtained. In the present work, it was used the standard value defined by DIANA. The multidirectional models present some differences in relation to the fixed models, among which it may be pointed out: different concrete models for tensile stresses, an option to decrease or not the transverse stiffness and the possibility to use constitutive models originated from the plasticity theory. The behavior of the concrete subjected to tensile stresses may be defined in two different forms: constant or linear:

- **Constant:** it admits a constant value of the tensile strength and considers the beginning of a crack if the maximum principal tensile stress exceeds the concrete tensile strength.
- **Linear:** it admits a linear variation and considers the beginning of new cracks, if the principal tensile stress exceeds the minimum value between f_t and $f_t(1 + \sigma_{lateral} / f_c)$, in which $\sigma_{lateral}$ is the principal lateral stress and f_c is the concrete compressive strength.

In the smeared crack models, it is adopted a reduction parameter β for the transverse stiffness of the material known as "shear retention factor". Thus, the shear stiffness may be expressed by:

$$D_{sec} = \frac{\beta}{1 - \beta} G \quad (4)$$

The parameter β may range from 0 to 1. For values next to zero, it is achieved a very small concrete shear stiffness and in the opposite case, for the unitary value it is obtained an infinite shear stiffness that will prevent the formation of cracks in this direction. Following the recommendations found in the literature, in the numerical examples analyzed in this work it was adopted $\beta = 0.2$. In the multidirectional smeared crack model it is possible to adopt a plasticity criterion for the material: Tresca, von Mises, Mohr-Coulomb or Drucker-Prager, and to choose the concrete tensile behavior in the softening branch. Among the different softening rules of the material available in DIANA it can be pointed out: brittle, linear, and non-linear by Moelands-Reinhardt and Hordijk, according to Figure 1.

The brittle behavior is characterized by the total reduction of stress after the failure criterion has been achieved. This behavior may be described by the following expression:

$$\frac{\sigma^{cr}(\epsilon^{cr})}{f_t} = \begin{cases} 1 \rightarrow & \epsilon^{cr} \leq 0 \\ 0 \rightarrow & 0 < \epsilon^{cr} < \infty \end{cases} \quad (5)$$

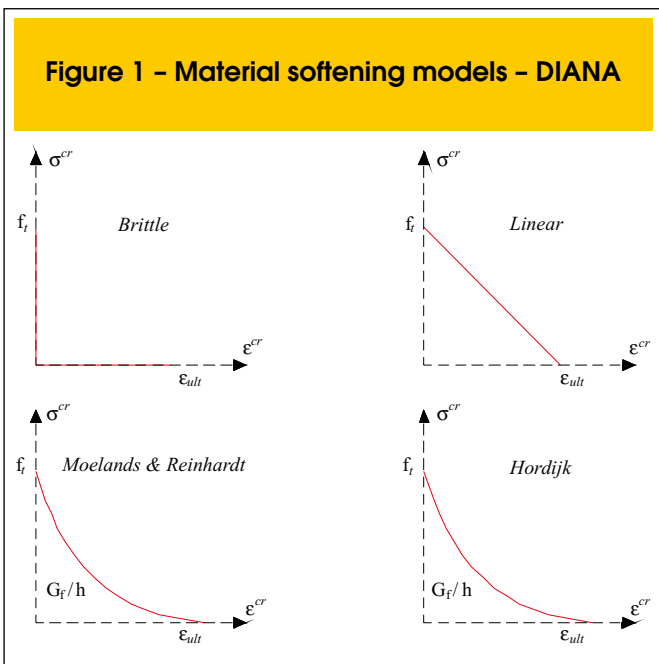
In the case of the linear softening model, the stress-strain relationship in the crack is defined by the following expression:

$$\frac{\sigma^{cr}(\epsilon^{cr})}{f_t} = \begin{cases} 1 - \frac{\epsilon^{cr}}{\epsilon_{ult}} \rightarrow & 0 < \epsilon^{cr} \leq \epsilon_{ult} \\ 0 \rightarrow & \epsilon_{ult} < \epsilon^{cr} < \infty \end{cases} \quad (6)$$

Two other non-linear models may still be adopted. The softening model by Moelands-Reinhardt uses a non-linear relationship between stresses and strains expressed in the following equation, with the coefficient c_1 taking the constant value of 0.31:

$$\frac{\sigma^{cr}(\epsilon^{cr})}{f_t} = \begin{cases} 1 - \left(\frac{\epsilon^{cr}}{\epsilon_{ult}} \right)^{c_1} \rightarrow & 0 < \epsilon^{cr} \leq \epsilon_{ult} \\ 0 \rightarrow & \epsilon_{ult} < \epsilon^{cr} < \infty \end{cases} \quad (7)$$

The other non-linear model present in DIANA is the model by Hordijk which uses an exponential relationship between the normal tensile



stresses and strains, with the coefficients c_1 and c_2 taking, respectively, the values of 3.0 and 6.93, according to the following equation:

$$\frac{\sigma^{cr}(\epsilon^{cr})}{f_t} = \begin{cases} \left(1 + \left(c_1 \frac{\epsilon^{cr}}{\epsilon_{ult}}\right)^3\right) \exp\left(-c_2 \frac{\epsilon^{cr}}{\epsilon_{ult}}\right) - \frac{\epsilon^{cr}}{\epsilon_{ult}} \left(1 + c_1^3\right) \exp(-c_2) \rightarrow 0 < \epsilon^{cr} \leq \epsilon_{ult} \\ 0 \rightarrow \epsilon_{ult} < \epsilon^{cr} < \infty \end{cases} \quad (8)$$

The multidirectional model available in DIANA is characterized for modeling the material combining a smeared crack model (brittle, linear, exponential,...) with a plastic model for compression, in which it is possible to use the classical failure models by Tresca, Von Mises, Mohr-Coulomb and Drucker-Prager.

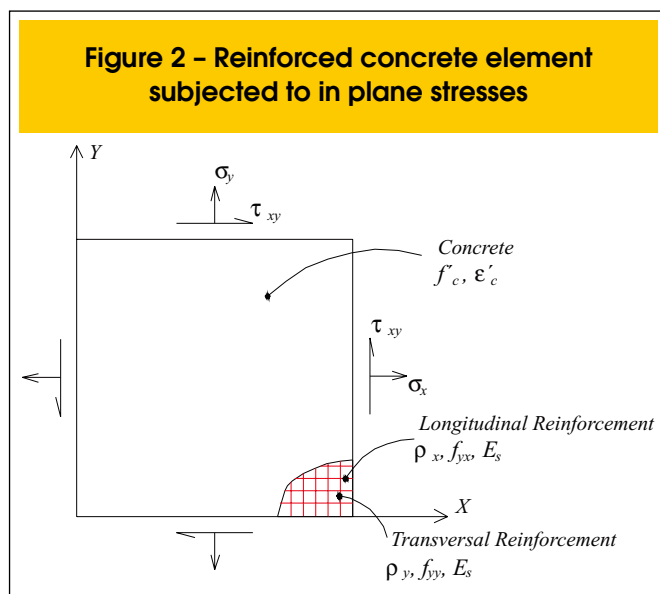
The constitutive model for the reinforcement is the perfect elasto-plastic. By adopting this model, the reinforcement stress may be determined by the equations (9) and (10), where f_y is the yield stress, E_s is the elastic module and ϵ_s is the reinforcement strain:

$$\sigma_s = \pm E_s \epsilon_s \quad \text{if} \quad -\epsilon_y \leq \epsilon_s \leq \epsilon_y \quad (9)$$

$$\sigma_s = \pm f_y \quad \text{if} \quad \epsilon_y \leq \epsilon_s \leq \epsilon_s^{ult} \quad \text{OR} \quad -\epsilon_s^{ult} \leq \epsilon_s \leq -\epsilon_y \quad (10)$$

4. Smeared crack models in VecTor2

VecTor2 is a finite element software used in the analysis of two-dimensional reinforced concrete structures which has been developed at the University of Toronto since 1990. The software development has been happening parallel to a series of experimental tests, in order to better predict the behavior of a variety of reinforced concrete structures.



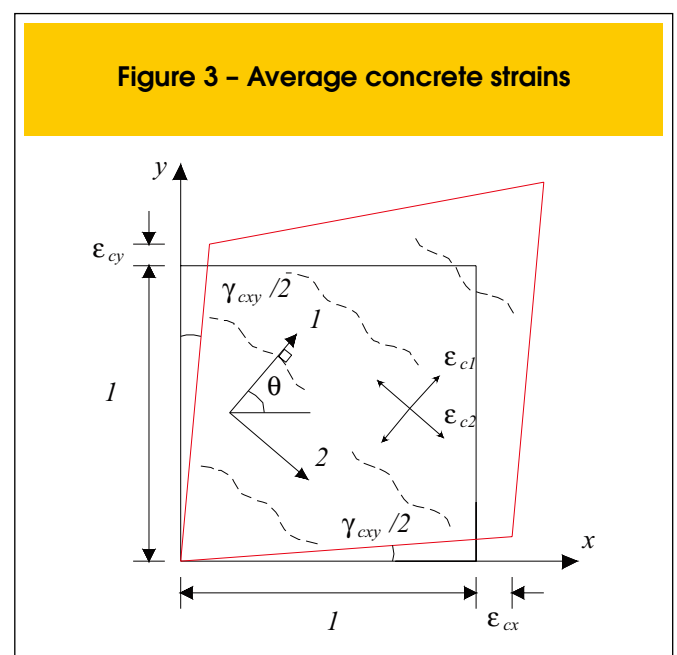
The theoretical bases of VecTor2 are the MCFT – Modified Compression Field Theory, developed by Vecchio and Collins [12] and DSFM – Disturbed Stress Field Model, developed later by Vecchio [4]. These formulations are analytical models to predict the response of reinforced concrete elements, representing the cracked concrete as an orthotropic material with rotating smeared cracks. The main concepts of the MCFT and DSFM formulations will be addressed in the next sections.

4.1 Modified Compression Field Theory (MCFT)

The MCFT is an analytical model to represent the behavior of two-dimensional reinforced concrete structures discretized by membrane elements subjected to normal and shear stresses, as shown in Figure 2.

This formulation evaluates the average stresses and strains (in the region between the cracks) and the local stresses and strains of the concrete and reinforcement, as well as the widths and orientations of the cracks during the loading and, based on this information, the failure mode of the element can be determined.

The modeling of the cracked concrete element is performed by using an orthotropic material and a rotating smeared crack model. In other words, the cracked concrete is treated like a continuous medium with cracks smeared across the membrane element. The smeared cracks may suffer changes in their directions always remaining linked to the direction changes in the principal stress field. The MCFT is based on three groups of relationships: compatibility relationships for the average strains in the concrete and reinforcement; equilibrium relationships for the average stresses in the concrete and reinforcement; and the constitutive relationships for the cracked concrete and reinforcement. Among the hypotheses admitted in the MCFT formulation, it may be pointed out: the uniformly distributed reinforcement; uniformly applied shear and normal stresses; perfect bond between the concrete and the reinforcement; uniformly distributed and rotating cracks; and the orientation of principal stress and strain are the same.



4.1.1 Compatibility relationships in the MCFT

The compatibility relationships in the MCFT are achieved from the average strains in the components which represent the concrete and the reinforcement, according to Figure 3. Based on the perfect bond hypothesis, the average strains in the concrete (ϵ_c) are equal to the average strains in the reinforcement (ϵ_s). Although any number of components and reinforcement orientations may be considered in the MCFT formulation, considering the membrane element orthogonally reinforced of Figure 2, the compatibility equations may be expressed by:

$$\epsilon_x = \epsilon_{cx} = \epsilon_{sx} \tag{11}$$

$$\epsilon_y = \epsilon_{cy} = \epsilon_{sy} \tag{12}$$

With a value for the shear strain γ_{xy} , it is possible to obtain the average principal concrete tensile strain (ϵ_{c1}) and the average principal concrete compressive (ϵ_{c2}), as well as the orientations of the average principal tensile strain and stress axes using Mohr's circle:

$$\epsilon_{c1}, \epsilon_{c2} = \frac{1}{2} \cdot (\epsilon_x + \epsilon_y) \pm \frac{1}{2} \left[(\epsilon_x - \epsilon_y)^2 + \gamma_{xy}^2 \right]^{0.5} \tag{13}$$

$$\theta = \theta_\epsilon = \theta_\sigma = \frac{1}{2} \cdot \tan^{-1} \left(\frac{\gamma_{xy}}{\epsilon_x - \epsilon_y} \right) \tag{14}$$

4.1.2 Equilibrium relationships in the MCFT

Considering the free body diagram of the membrane element shown in Figure 4, through the balance of forces in the x and y directions, the results of the normal stresses applied in panel σ_x e σ_y must be balanced by the normal stresses in the concrete f_{cx} and f_{cy} and by the stresses in the reinforcement f_{sx} e f_{sy} . The balance of moments requires that the shear stress applied to the panel, represented by τ_{xy} , to be totally resisted by the average shear stress in the concrete τ_{cxy} , assuming that the reinforcement does not present any kind of dowel action. Thus, these equilibrium relationships for the average stresses may be expressed by the following equations, where ρ_{sx} and ρ_{sy} are the reinforcement ratios in the x and y directions:

$$\sigma_x = f_{cx} + \rho_{sx} f_{sx} \tag{15}$$

$$\sigma_y = f_{cy} + \rho_{sy} f_{sy} \tag{16}$$

$$\tau_{xy} = \tau_{cxy} \tag{17}$$

Since the cracked concrete is orthotropic with respect to the directions of the principal stress, Mohr's circle can be used to relate the average concrete stresses f_{cx} and f_{cy} , to the average principal concrete tensile stress f_{c1} :

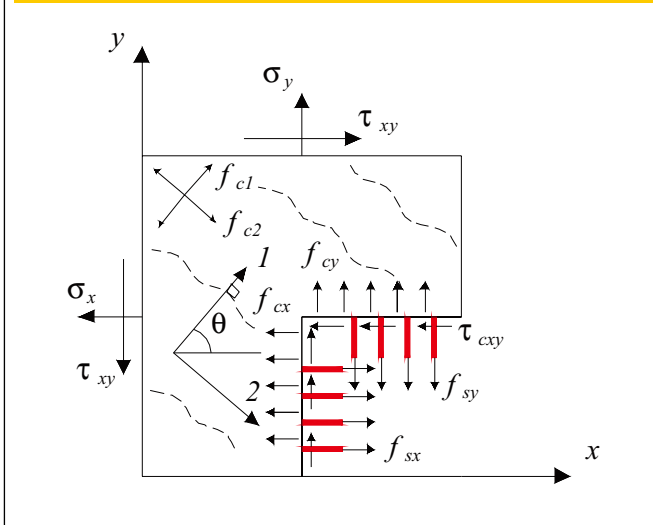
$$f_{cx} = f_{c1} - \tau_{cxy} / \tan(\theta) \tag{18}$$

$$f_{cy} = f_{c1} - \tau_{cxy} \cdot \tan(\theta) \tag{19}$$

4.1.3 Constitutive relationships in the MCFT

A set of thirty panels measuring 890x890x70 mm was tested experimentally and the results were analyzed to develop constitutive models able to represent the behavior of the cracked concrete in compression and tension. The constitutive relationship to describe the concrete in com-

Figure 4 - Free body diagram of the reinforced concrete element



pression relates the principal compressive stress, f_{c2} , to the principal compressive strain, ϵ_{c2} . The tests with the panels have indicated that the compressive strength and stiffness suffered reductions as the principal tensile strain, ϵ_{c1} increased. This phenomenon, known as compression softening is incorporated through the stiffness reduction in the stress-strain curve of the concrete:

$$f_{c2} = \frac{f_c' (2(\epsilon_{c2} / \epsilon_0) - (\epsilon_{c2} / \epsilon_0)^2)}{0.8 - 0.34(\epsilon_{c1} / \epsilon_0)} \quad (20)$$

The term which appears in the numerator is the Hognestad's parabolic relationship, obtained for the concrete subjected to the uniaxial compression, generally used for normal strength concrete. The value ϵ_0 corresponds to the strain associated to the peak stress of the concrete f_c' , as determined experimentally from uniaxial compression tests of concrete cylinders. The denominator reflects the softening effect. With regards to concrete in tension, it is first necessary to determine the values of the uniaxial cracking strength of the concrete, f_t' , and its corresponding tensile strain, ϵ_{cr} , which may be obtained through the following expressions:

$$f_t' = 0.33\sqrt{f_c'} \quad (\text{MPa}) \quad (21)$$

$$\epsilon_{cr} = \frac{f_t'}{E_c} \quad (22)$$

where E_c is the initial tangent stiffness of the concrete, estimated by the following expression:

$$E_c = 5000\sqrt{f_c'} \quad (\text{MPa}) \quad (23)$$

It is admitted that before cracking, the concrete presents a linear-elastic behavior in tension. Therefore, after cracking, tensile stresses may continue to exist in the concrete between the cracks due to bond interactions between the concrete and reinforcement. To model this phenomenon known as *tension stiffening*, the MCFT proposed the following relationship:

$$f_{c1} = E_c \epsilon_{c1} \quad \text{for} \quad 0 < \epsilon_{c1} \leq \epsilon_{cr} \quad (24)$$

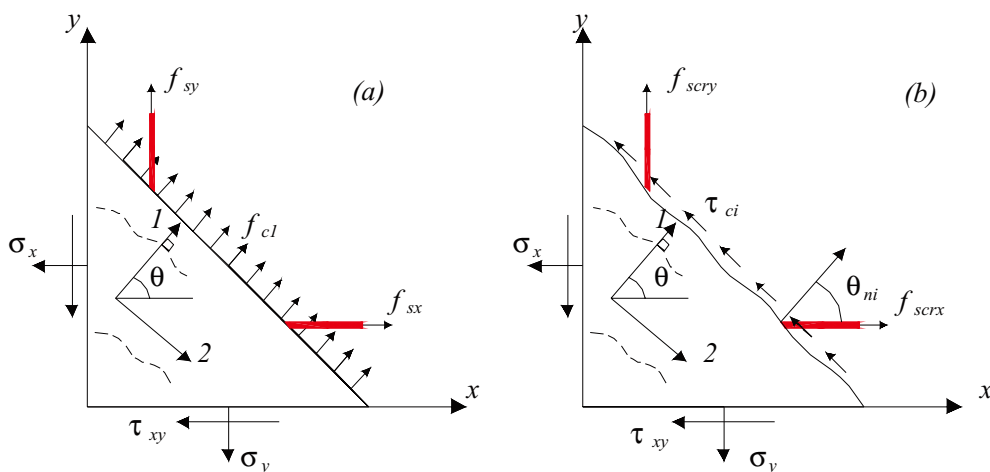
$$f_{c1} = \frac{f_t'}{1 + \sqrt{200\epsilon_{c1}}} \quad \text{for} \quad \epsilon_{c1} > \epsilon_{cr} \quad (25)$$

For the reinforcement in compression and tension, the MCFT uses a bilinear relationship to relate the average stress and strain, in the same way it had been done with the crack model in DIANA.

$$f_s = E_s \epsilon_s \leq f_s^{yield} \quad (26)$$

where E_s is the elastic module and f_s^{yield} is the yield stress of the reinforcement.

Figure 5 - (a) Average stresses between cracks and (b) local stresses at crack free surface



4.1.4 Local crack conditions in the MCFT

Given a compatible average strain condition, the constitutive relationships can be used to determine the average stresses in the concrete and reinforcement, as well as the normal and shear stresses acting on the structure. However, it would be unconservative to disregard the possibility that the response of the structure may be guided by the local yielding of the reinforcement at the crack or sliding shear failure along a crack. To cover these possibilities, the MCFT limits the local stresses at the crack and average tensile concrete stress.

The stress field in the reinforced concrete suffers variations when evaluated according to the average values in the area between the cracks and when evaluated locally at the crack. This behavior can be better understood considering Figure 5(a), which depicts the average stresses in a section located between cracks, and Figure 5(b), which depicts the local stresses at the free surface of the crack.

At a free surface of the crack, the average concrete tensile stresses are practically reduced to zero. Consequently, to transmit the average tensile stresses across the crack, the stresses and strains in the reinforcement must increase locally at the crack. Static equivalence between the average and local stresses in the normal direction to the crack surface, results in the following relationship:

$$f_{cl} = \rho_x (f_{scrx} - f_{sx}) \cos^2 \theta_{nx} + \rho_y (f_{scry} - f_{sy}) \cos^2 \theta_{ny} \quad (27)$$

where f_{scrx} and f_{scry} are the local reinforcement stresses at a crack, and θ_{nx} and θ_{ny} the values of the angles between the normal to the crack and the reinforcement. Considering the equation (27), the average tensile concrete stress must be limited by the yielding of the reinforcement at the crack and consequently:

$$f_{cl} \leq \rho_x (f_{sxyield} - f_{sx}) \cos^2 \theta_{nx} + \rho_y (f_{syyield} - f_{sy}) \cos^2 \theta_{ny} \quad (28)$$

As a principal plane, the shear stress is absent and thus, they do not appear in Figure 5(a). However, as the reinforcement generally crosses the cracks at a skew angle, the local shear stresses, τ_{ci} will be present on the crack surface. Consequently, through the static equivalence of the average and local stresses in the tangential direction to the surface of the crack, the local shear stresses can be determined by the following equation:

$$\tau_{ci} = \rho_x (f_{scrx} - f_{sx}) \cos(\theta_{nx}) \sin(\theta_{nx}) + \rho_y (f_{scry} - f_{sy}) \cos(\theta_{ny}) \sin(\theta_{ny}) \quad (29)$$

However, the local shear stress is limited by the aggregate interlock mechanism, which decreases with the increase of the crack width (w) and with the reduction of the size of the aggregated (a). Based on the analysis of the aggregate interlock mechanisms developed

by Walraven [13], the MCFT establishes a limit for the shear stress on the crack:

$$\tau_{ci} \leq \frac{0.18 \sqrt{f'_c}}{0.31 + 24w/(a + 26)} \quad (30)$$

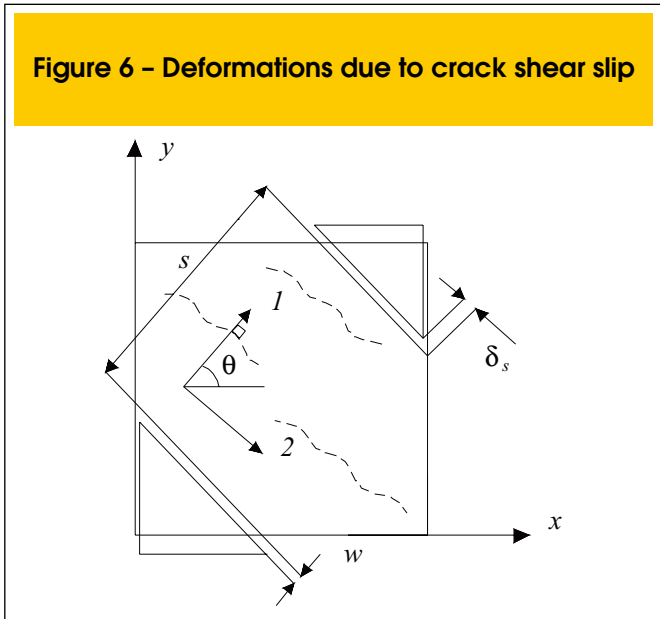
4.2 Disturbed Stress Field Model (DSFM)

The DSFM is an extension of the MCFT, with the purpose of treating the MCFT deficiencies. For example, in lightly reinforced elements, in which the shear slip along the crack is more expressive, the rotation of the stress field tends to present a certain discrepancy concerning the rotation of the strain field. In these cases, the stiffness and strength end up being overestimated by the MCFT, which assumes the orientations of the principal stress and strain are the same. On the other hand, in elements which present small rotations in the stress and strain fields, the MCFT generally underestimates the shear stiffness and strength.

The DSFM is conceptually similar to the MCFT, however, it ends up extending the MCFT in several aspects. Primarily, the DSFM enlarges the compatibility relationships of the MCFT to include crack shear slip. Furthermore, the DSFM decouples the orientation of the principal stress and strain fields. By explicitly calculating crack slip deformations, the DSFM eliminates the need to check the shear stress. Modifications in the calculation of the constitutive relationships for the concrete and reinforcement are also presented.

4.2.1 Compatibility relationships in the DSFM

Although the MCFT admits that the orientations of the principal stresses and strains remain the same, experimental tests indicate that this hypothesis is not always valid after the crack. The experimental results show that the principal strain field generally suffers modifications in its orientation at a larger rate than in the principal stress field.



This phenomenon is attributable to the manner by which the stress and strain fields are determined. The measured strains are total strains, which are obtained by the sum of the average strains in cracked concrete (Figure 2) and the shear strains, caused by slipping across the crack, as shown in Figure 6.

In order to represent this behavior, the DSFM defines the total strains, ϵ_x , ϵ_y and γ_{xy} as the sum of the net concrete strains, ϵ_{cx} , ϵ_{cy} and γ_{cxy} , and the strains due to shear slip, ϵ_x^s , ϵ_y^s and γ_{xy}^s .

$$\epsilon_x = \epsilon_{cx} + \epsilon_x^s \quad (31)$$

$$\epsilon_y = \epsilon_{cy} + \epsilon_y^s \quad (32)$$

$$\gamma_{xy} = \gamma_{cxy} + \gamma_{xy}^s \quad (33)$$

The principal net concrete tensile strain (ϵ_{c1}) and principal net concrete compressive strain (ϵ_{c2}) may be evaluated using Mohr's circle:

$$\epsilon_{c1}, \epsilon_{c2} = \frac{1}{2} \cdot (\epsilon_{cx} + \epsilon_{cy}) \pm \frac{1}{2} \left[(\epsilon_{cx} - \epsilon_{cy})^2 + \gamma_{cxy}^2 \right]^{0.5} \quad (34)$$

The crack slip shear components, ϵ_x^s , ϵ_y^s and γ_{xy}^s , can be calculated from the average crack slip shear strain γ_c . This strain is equal to the slip in the crack, δ_s , divided by the average space between the cracks, s , according to the following expression:

$$\gamma_s = \frac{\delta_s}{s} \quad (35)$$

$$\epsilon^s = \begin{Bmatrix} \epsilon_x^s \\ \epsilon_y^s \\ \gamma_{xy}^s \end{Bmatrix} = \begin{Bmatrix} -\frac{1}{2} \gamma_s \cdot \sin(2\theta) \\ \frac{1}{2} \gamma_s \cdot \sin(2\theta) \\ \gamma_s \cdot \cos(2\theta) \end{Bmatrix} \quad (36)$$

The orientation of the principal net concrete strains, θ , and the orientation of the principal concrete stress, θ_σ , with respect to the x axis can be determined from Mohr's circle with the components of the net concrete strain as follows:

$$\theta = \theta_\sigma = \frac{1}{2} \cdot \tan^{-1} \left(\frac{\gamma_{cxy}}{\epsilon_{cx} - \epsilon_{cy}} \right) \quad (37)$$

Likewise, the orientation of the principal total strain field, θ_ϵ , can be determined from the components of the total strain:

$$\theta_\epsilon = \frac{1}{2} \cdot \tan^{-1} \left(\frac{\gamma_{xy}}{\epsilon_x - \epsilon_y} \right) \quad (38)$$

Although in the DSFM, it is possible to use any number of reinforcement components and orientations, considering the orthogonally reinforced membrane element and assuming perfect bond, the average strains in the components of the reinforcement in the x and y directions will be equal to the total strains:

$$\epsilon_{sx} = \epsilon_x \quad (39)$$

$$\epsilon_{sy} = \epsilon_y \quad (40)$$

4.2.2 Equilibrium relationships in the DSFM

Considering again an orthogonally reinforced membrane element, the equilibrium relationships of the DSFM are the same determined previously for the MCFT, that is:

$$\sigma_x = f_{cx} + \rho_{sx} f_{sx} \quad (41)$$

$$\sigma_y = f_{cy} + \rho_{sy} f_{sy} \quad (42)$$

$$\tau_{xy} = \tau_{cxy} \quad (43)$$

Similarly, the DSFM formulation also incorporates the equilibrium relationships for the local stresses at the crack:

$$f_{cl} = \rho_x (f_{scrx} - f_{sx}) \cos^2 \theta_{nx} + \rho_y (f_{scry} - f_{sy}) \cos^2 \theta_{ny} \quad (44)$$

$$\tau_{ci} = \rho_x (f_{scrx} - f_{sx}) \cos(\theta_{nx}) \cdot \sin(\theta_{nx}) + \rho_y (f_{scry} - f_{sy}) \cos(\theta_{ny}) \cdot \sin(\theta_{ny}) \quad (45)$$

It is worthy pointing out that the average concrete tensile stress must be limited by the yielding of the reinforcement traversing the crack:

$$f_{cl} \leq \rho_x (f_{sxyield} - f_{sx}) \cos^2 \theta_{nx} + \rho_y (f_{syyield} - f_{sy}) \cos^2 \theta_{ny} \quad (46)$$

However, unlike the MCFT, the tensile stress is not subjected to the limitation of the shear stresses at a crack, since the DSFM incorporates deformations due to shear slip, instead of imposing a limit stress corresponding to the shear slip failure.

4.2.3 Constitutive relationships in the DSFM

The experimental analysis of a series of reinforced concrete panels led Vecchio and Collins [12] to propose a reduction factor, β_d , in order to reflect the softening effect of the concrete and its connection to the principal tensile strain.

$$\beta_d = \frac{1}{1 + C_s C_d} \leq 1.0 \quad (47)$$

In this equation, the softening effect of transverse tensile strains is taken into account by factor C_d , defined by:

$$C_d = 0.35 \left(-\varepsilon_{cl} / \varepsilon_{c2} - 0.28 \right)^{0.8} \quad (48)$$

The factor C_s determines if the analysis of the element will take into account slip deformations. If the analysis does not consider the slip deformations, as in the MCFT, then factor $C_s = 1.0$. If the analysis considers element slip distortions, as in the DSFM, then the softening effect appears to be less for the same value of the relationship $\varepsilon_{cl} / \varepsilon_{c2}$ since the softening effect is attributed only to the tensile strains and in this case, $C_s = 0.55$.

In order to consider the concrete softening effect, the concrete cylinder strength f'_c , and its corresponding strain peak, ε'_c , are both reduced:

$$f_p = -\beta_d \cdot f'_c \quad (49)$$

$$\varepsilon_p = -\beta_d \cdot \varepsilon'_c \quad (50)$$

With regards to the constitutive models to simulate the behavior of the concrete in tension, it is admitted that the response before crack is linear-elastic and for cracked concrete the average concrete tensile stresses, f_{cl}^a , due to tension stiffening, may be modeled by a nonlinearly decaying relationship:

$$f_{cl} = E_c \varepsilon_{cl} \quad , \quad 0 \leq \varepsilon_{cl} \leq \varepsilon_{cr} \quad (51)$$

$$f_{cl}^a = \frac{f_t'}{1 + \sqrt{c_t \varepsilon_{cl}}} \quad , \quad \varepsilon_{cl} > \varepsilon_{cr} \quad (52)$$

The coefficient c_t incorporates the influence of the reinforcement bond characteristics and can be determined by the following equation:

$$c_t = 2.2m \quad (53)$$

$$\frac{1}{m} = \sum_{i=1}^n \frac{4\rho_i}{d_{bi}} |\cos \theta_{mi}| \quad (\text{mm}) \quad (54)$$

where d_{bi} is the bar diameter and ρ_i is the reinforcement ratio of each of the n reinforcement components. In the DSFM, a trilinear constitutive model for reinforcement in tension or compression is used to account for strain-hardening phenomenon:

$$f_s = E_s \varepsilon_s \quad , \quad 0 < \varepsilon_s \leq \varepsilon_{syield} \quad (55)$$

$$f_s = f_{syield} \quad , \quad \varepsilon_{syield} < \varepsilon_s \leq \varepsilon_{sh} \quad (56)$$

$$f_s = f_{yield} + E_{sh} (\epsilon_s - \epsilon_{sh}) , \quad \epsilon_{sh} < \epsilon_s \leq \epsilon_u \quad (57)$$

where E_s is the elastic module; f_{yield} is the yield strength of the reinforcement; ϵ_{yield} is the yield strain of the reinforcement; ϵ_{sh} is the strain at the onset of strain hardening; and ϵ_u is the ultimate strain of the reinforcement.

4.3 Composite material stiffness matrix

The composite material stiffness matrix is the sum of the concrete material stiffness matrix D_c and the reinforcement component material stiffness matrices D_{si} :

$$D = D_c + \sum_{i=1}^n D_{si} \quad (58)$$

As the MCFT and DSFM model the reinforced concrete element as an orthotropic material in the principal stress direction, it is necessary to formulate the concrete material stiffness matrix relative to these directions, D_c' . Assuming that the Poisson's effect is negligible, then D_c' can be calculated by:

$$D_c' = \begin{bmatrix} \bar{E}_{c1} & 0 & 0 \\ 0 & \bar{E}_{c2} & 0 \\ 0 & 0 & \bar{G}_c \end{bmatrix} \quad (59)$$

The secant modules are computed from the current values of the principal stresses f_{c1} and f_{c2} and the corresponding net concrete strains ϵ_{c1} and ϵ_{c2} :

$$\bar{E}_{c1} = \frac{f_{c1}}{\epsilon_{c1}} , \quad \bar{E}_{c2} = \frac{f_{c2}}{\epsilon_{c2}} , \quad \bar{G}_c = \frac{\bar{E}_{c1} \cdot \bar{E}_{c2}}{\bar{E}_{c1} + \bar{E}_{c2}} \quad (60)$$

Likewise, the reinforcement component matrices D_{si}' must be determined initially relative to their longitudinal axes. Assuming that the reinforcement only resists to uniaxial stresses, the matrix D_{si}' can be determined by:

$$D_{si}' = \begin{bmatrix} \rho_i \bar{E}_{si} & 0 & 0 \\ 0 & 0 & 0 \\ 0 & 0 & 0 \end{bmatrix} \quad (61)$$

$$\bar{E}_{si} = \frac{f_{si}}{\epsilon_{si}} \quad (62)$$

Afterwards, the material stiffness matrices D_c' and D_{si}' initially evaluated relative to the principal axes are transformed to the x and y axes by means of the transformation matrix:

$$D_c = T_c^T \cdot D_c' \cdot T_c \quad (63)$$

$$D_{si} = T_{si}^T \cdot D_{si}' \cdot T_{si} \quad (64)$$

$$T = \begin{bmatrix} \cos^2 \psi & \sin^2 \psi & \cos \psi \cdot \sin \psi \\ \sin^2 \psi & \cos^2 \psi & -\cos \psi \cdot \sin \psi \\ -2 \cos \psi \cdot \sin \psi & 2 \cos \psi \cdot \sin \psi & \cos^2 \psi - \sin^2 \psi \end{bmatrix} \quad (65)$$

5. Numerical examples

5.1 Simply supported reinforced concrete beam – Leonhardt and Walther [14]

A set of four reinforced concrete beams (ET1, ET2, ET3 e ET4) experimentally analyzed by Leonhardt and Walther [14] will be studied numerically using different smeared crack models in DIANA and VecTor2. The beams are simply supported and submitted to vertical loads as shown in Figure 7.

The beams have the same amount of reinforcement but they have different core widths, what implies in different reinforcement ratios.

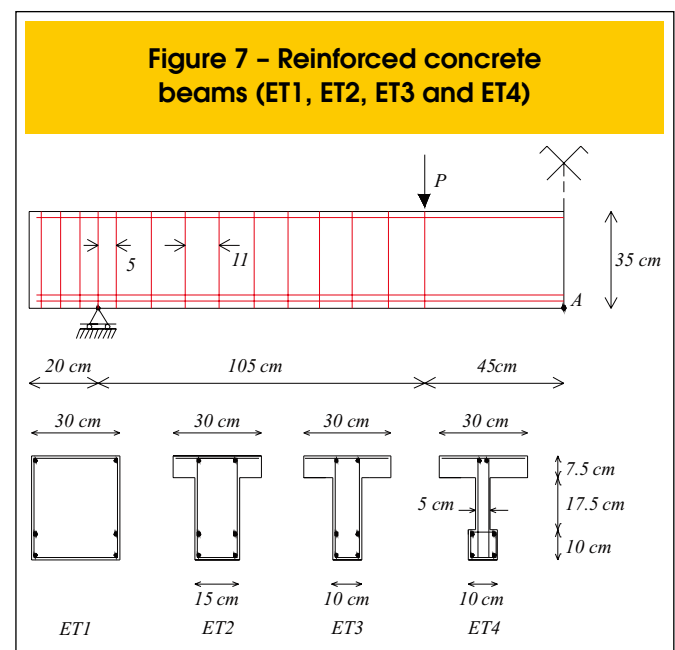


Table 1 - Mechanical properties for cracked concrete

Property	Value	Softening Models
Shear Retention factor (β)	0.2	All DIANA models
Ultimate Strain(ϵ_u)	0.0003337	Linear
Fracture Energy (G_f)	0.00068 KN/cm	Moelands-Reinhardt, Hordijk
Crack bandwidth (h)	17.32 cm	Moelands-Reinhardt, Hordijk

The longitudinal reinforcement at the bottom of the cross section consists of four bars with diameter of 20 mm and yield stress $f_y = 428 \text{ MPa}$. The longitudinal reinforcement at the top consists of two bars with diameter of 8 mm and yield stress $f_y = 465 \text{ MPa}$. The transverse reinforcement is represented by stirrups of 6 mm and yield stress $f_y = 320 \text{ MPa}$.

The concrete cube strength, achieved experimentally by Leonhardt and Walther [14], was $f_{cub} = 28.5 \text{ MPa}$. The corresponding values for the concrete cylinder strength ($f_c = 22.8 \text{ MPa}$), the concrete cracking strength ($f_t = 1.57 \text{ MPa}$) and the initial elastic module ($E_{co} = 23874.67 \text{ MPa}$) were determined from the concrete cube strength, according to Vecchio and Collins [12].

The set of reinforced concrete beams was analyzed with smeared crack models, employing different softening rules from DIANA (brittle, linear, non-linear by Moelands-Reinhardt and Hordijk) and the plasticity criterion by von Mises, as well as using the DSFM from VecTor2. The parameters used in the softening models are showed in Table 1. The perfect elasto-plastic behavior and elastic module $E_s = 210000 \text{ MPa}$ were considered for the reinforcements.

The finite element mesh used for modeling the concrete structure with 341 nodes and 300 rectangular elements is shown in Figure 8. Incorporated models were used in DIANA for the discretization of the reinforcement. On the other hand, VecTor2 used discrete models for the longitudinal reinforcement and smeared models for the stirrups.

The vertical displacements of the beams at Point A (midspan) are shown in Figure 9. It can be observed that the load x displacement curves achieved with the different models present a great concordance with the experimental results. In general, the computational models presented a little higher stiffness than the experimental results.

The additional stiffness associated to the consideration of perfect bond and the contribution of concrete between cracks is more significant for smaller reinforcement ratios. The beam ET1 (with the smaller reinforcement ratio) presented the biggest discrepancy to the experimental results. The discrepancy between numerical and experimental models was less significant in the beams with higher reinforcement ratios (ET2, ET3 and ET4), as according to d'Avila [15].

To better understand the behavior of the beams and their collapse mechanisms, it is shown in Figure 10, the crack pattern and the orientations of the principal tensile strains ϵ_1 and principal compressive strain ϵ_2 of the beam ET4 for a load $P=76.8 \text{ KN}$.

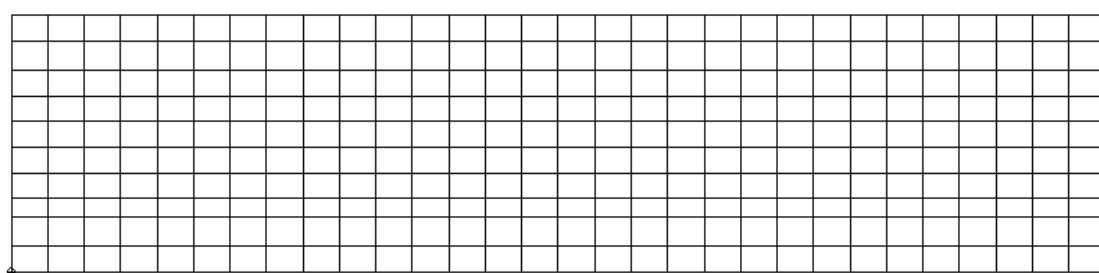
5.2 Continuous reinforced concrete beam – Leonhardt and Walther [16]

A set of three reinforced concrete beams (HH3, HH4, and HH5) tested experimentally by Leonhardt and Walther [16] will be analyzed using a smeared crack model with the softening rule by Hordijk and the plasticity criterion by von Mises in DIANA and also with the DSFM in VecTor2. The beams have rectangular cross sections ($25 \times 32 \text{ cm}^2$), presenting different lengths and reinforcement ratios, as shown in Figure 11.

The positive and negative longitudinal reinforcements are represented by bars of 14 mm with yield stress $f_y = 417 \text{ MPa}$. The transverse reinforcements consist of stirrups of 8 mm with yield stress $f_y = 371 \text{ MPa}$.

The length of the beams and their respective mechanical properties are shown in Table 2. Likewise the previous example, the concrete cylinder strength, the concrete cracking strength and

Figure 8 - Finite element mesh - 10x30



the initial elastic module were determined from the concrete cube strength according to Vecchio and Collins [12].

The parameters adopted for the Hordijk's model are showed in Table 3. The perfect elasto-plastic behavior and elastic module $E_s = 210000 \text{ MPa}$ were adopted for the reinforcement.

The finite element mesh used for modeling the concrete structure with 369 nodes and 320 rectangular elements is shown in Figure 12. Incorporated models were used in DIANA for the discretization of the reinforcement. On the other hand, VecTor2 used discrete models for the longitudinal reinforcement and smeared models for the stirrups.

The vertical displacements of the beams at Point A are shown in Figure 13. The *load x displacement* curves achieved with the different models present a great concordance with the experimental results. At the beginning of the loading process the computational

models presented a smaller stiffness than the experimental results, however, for the final phase, this situation inverts and the computational models start to present a little higher stiffness than the experimental results.

The additional stiffness in the computational models is caused by two factors: the consideration of the perfect bond and the contribution of concrete between cracks, which was also observed in the previous example.

For this series of continuous beams, it is also showed a comparison of the reinforcement stresses for the different models. The analyzed points are: under the load for the positive reinforcement (Point C) and at the central support for the negative reinforcement (Point B), as shown in Figure 14, indicating that the computational models were able to evaluate properly the reinforcement stresses during the loading process.

Figure 9 - Load x Displacement curve (ET1, ET2, ET3 and ET4)

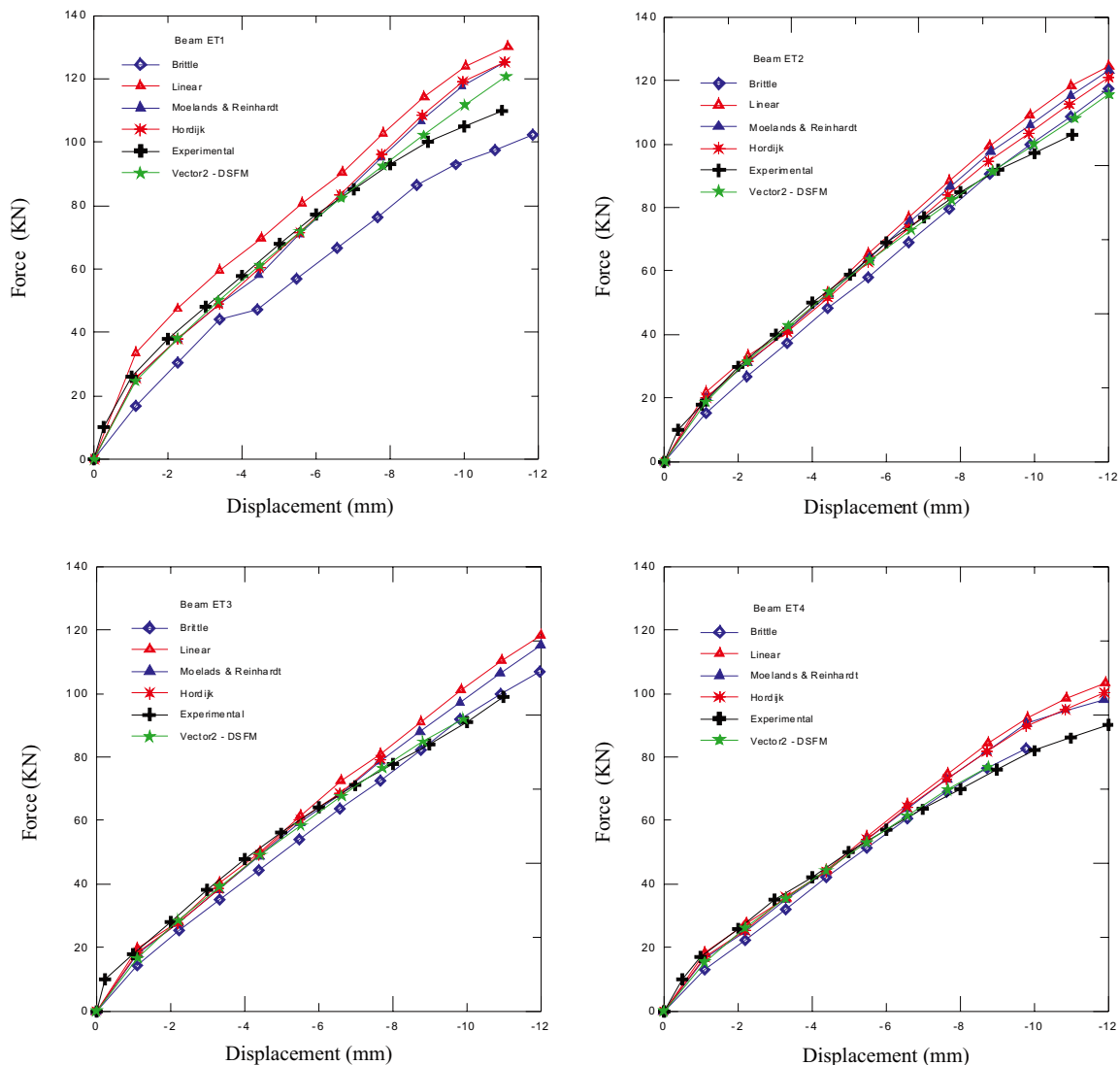


Figure 10 - Beam ET4 - (a) Deformed shape and beam crack pattern, (b) and (c) Orientations of the principal tensile and compressive strains ϵ_1 and ϵ_2

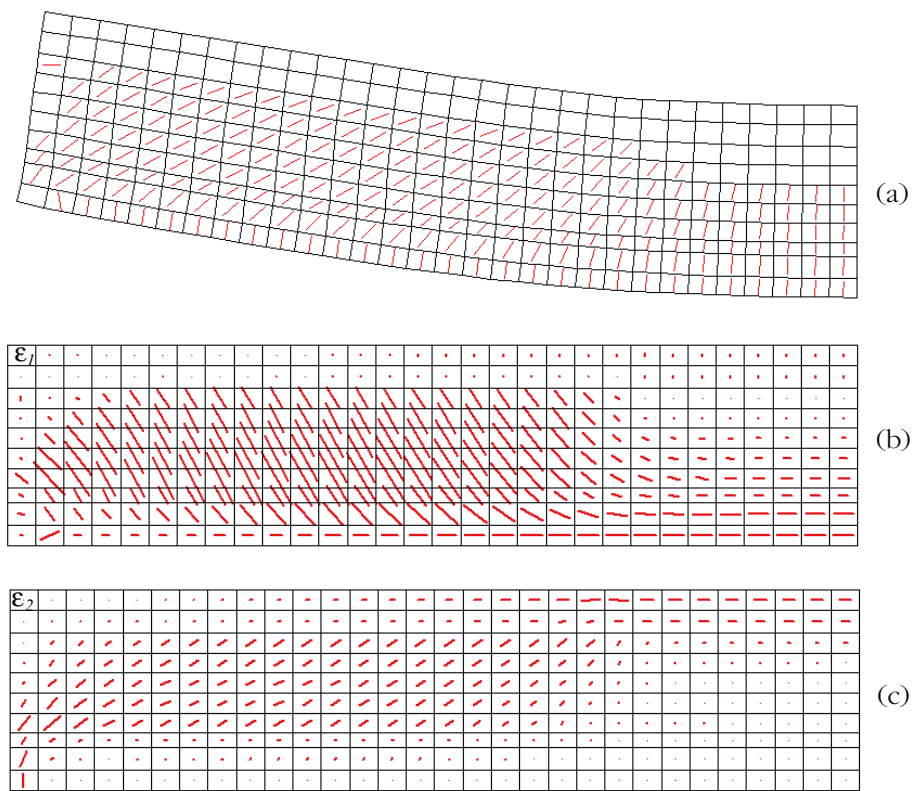


Figure 11 - Reinforced concrete beams (HH3, HH4 and HH5)

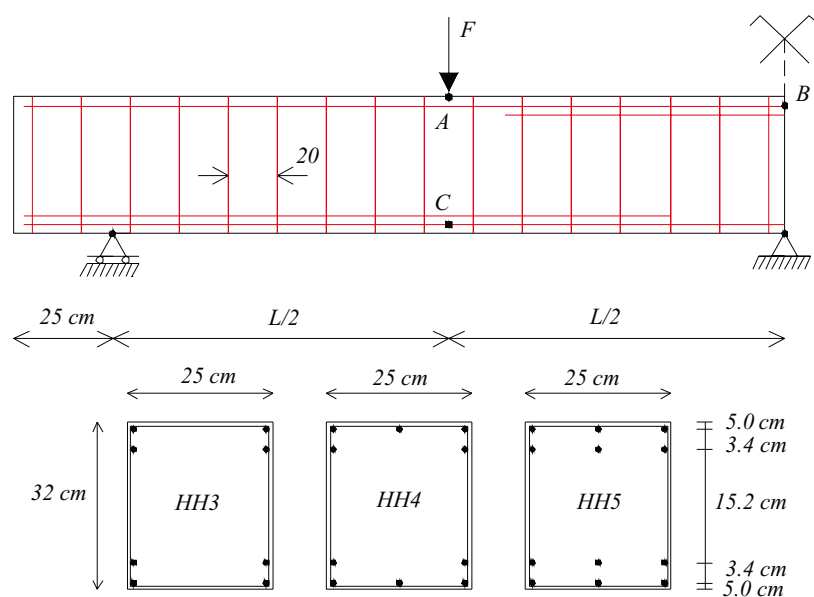


Table 2 - Mechanical properties of concrete

Beams	L (cm)	F_{cub} (MPa)	F_c (MPa)	F_t (MPa)	E_{c0} (MPa)
HH3	211	37.1	29.68	1.80	27240
HH4	257	33.6	26.88	1.71	25923
HH5	300	36.3	29.04	1.78	26944

Table 3 - Parameters for the Hordijk model

Property	Value	Beams
Shear Retention factor (β)	0.2	HH3, HH4 e HH5
Fracture Energy (G_f)	0.00068 KN/cm	HH3, HH4 e HH5
Crack bandwidth (h)	17.32 cm	HH3, HH4 e HH5

To better understand the behavior of the beams and their collapse mechanism, the crack pattern and the reinforcement stresses of the beam HH5 for a load $P=195.4$ KN are shown in Figures 15 and 16.

6. Conclusions

The smeared crack models of DIANA and VecTor2 proved to be very efficient to analyze the reinforced concrete beams subjected to bending. The *load x displacement* curves obtained with the different models presented a great concordance with the experimental values. In general, the computational models presented a higher stiffness than the experimental results. Among the causes of the additional stiffness, it can be pointed out the concrete contribution between cracks, which proved to be more significant for smaller reinforcement rates and the hypothesis of perfect bond, since due to the non-consideration of the bond loss, it is natural that the cracked structure becomes stiffer. The selection of the material softening rule showed to be more significant for smaller reinforcement ratios, in which the brittle model presented the highest discrepancy with respect to the experimental values.

The smeared crack models permitted to simulate the post-crack behavior of the reinforced concrete allowing to follow up the evolution of stresses and strains during the loading process and to obtain a crack pattern which enabled to better understand its be-

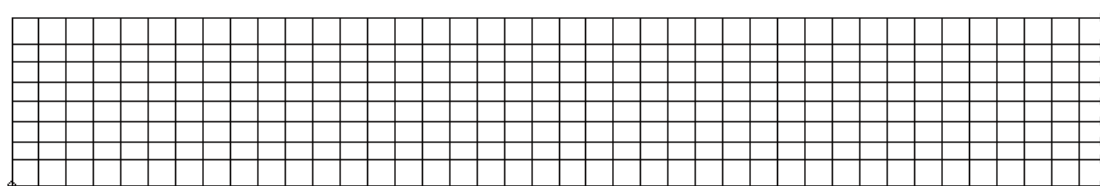
havior, as well as to follow up the stress evolutions and the yielding of the reinforcements.

7. Acknowledgments

The authors acknowledge the financial support from FAPESP and Professor Frank Vecchio from University of Toronto for the release of the use license for VecTor2.

8. References

- [01] Cedolin, L. e Dei Poli, S. Finite Element Studies of Shear-Critical R/C Beams. Journal of Engineering Mechanics Division, New York: ASCE, v.103, n.EM3, 1977; p.395-410.
- [02] Bazant, Z.P. e Gambarova, P. Rough Cracks in Reinforced Concrete. Journal of the Structural Division, New York: ASCE, v.106, 1980; p.819-842.
- [03] Gupta, A.K. e Maestrini, S.R. Post-Cracking Behavior of Membrane Reinforced Concrete Elements Including Tension-Stiffening. Journal of Structural Engineering. New York: ASCE, v.115, n.4, 1989; p.957-976.
- [04] Vecchio, F. Disturbed Stress Field Model for Reinforced Concrete: Formulation, ASCE, Journal

Figure 12 - Finite element mesh - 8x40

- of Structural Engineering, v.126, n.9, 2000; p.1070-1077.
- [05] Bazant, Z.P. e Cedolin, L. Finite Element Modeling of Crack Band Propagation. Journal of Structural Engineering, New York: ASCE, v.109, n.1, 1983; p.69-92.
- [06] Bazant, Z.P. e Oh, B. Crack Band Theory for Fracture Concrete. Materials & Constructions, v.16, n.93, 1983; p.155-177.
- [07] Feenstra, P.H. e de Borst, R. Constitutive Model for Reinforced Concrete. Journal of Engineering Mechanics, New York: ASCE, v.121, n.5, 1995; p.587-595.
- [08] Rots, J.G. e Blaauwendraad, J. Crack Models for Concrete: Discrete or Smeared? Fixed, Multi-directional or Rotating? HERON, Delft, v.34, n.1, 1989.
- [09] Ottosen, N.S. Material Models for Concrete, Steel and Concrete-Steel Interaction. Bulletin d'Information, n.194, Lausanne: CEB, 1988.
- [10] Pramono, E. e Willam, K. Fracture Energy-Based Plasticity Formulation of Plain Concrete. Journal of Engineering Mechanics, New York: ASCE, v.115, n.6, 1989; p.1183-1204.
- [11] COMITÉ EURO-INTERNATIONAL DU BÉTON. CEB-FIP Model Code 1990, Bulletin d'Information n.213/214, Lausanne: CEB, 1993.
- [12] Vecchio, F.J. e Collins, M.P. The Modified Compression Field Theory for Reinforced Concrete Elements Subject to Shear, ACI Journal, v.83, n.2, 1986; pp. 219-231.
- [13] Walraven, J.C. Fundamental Analysis of Aggregate Interlock, ASCE: Journal of the Structural Division, v. 107, n. 11, 1981; pp. 2245-2270.

Figure 13 – Load x Displacement curve (HH3, HH4 and HH5)

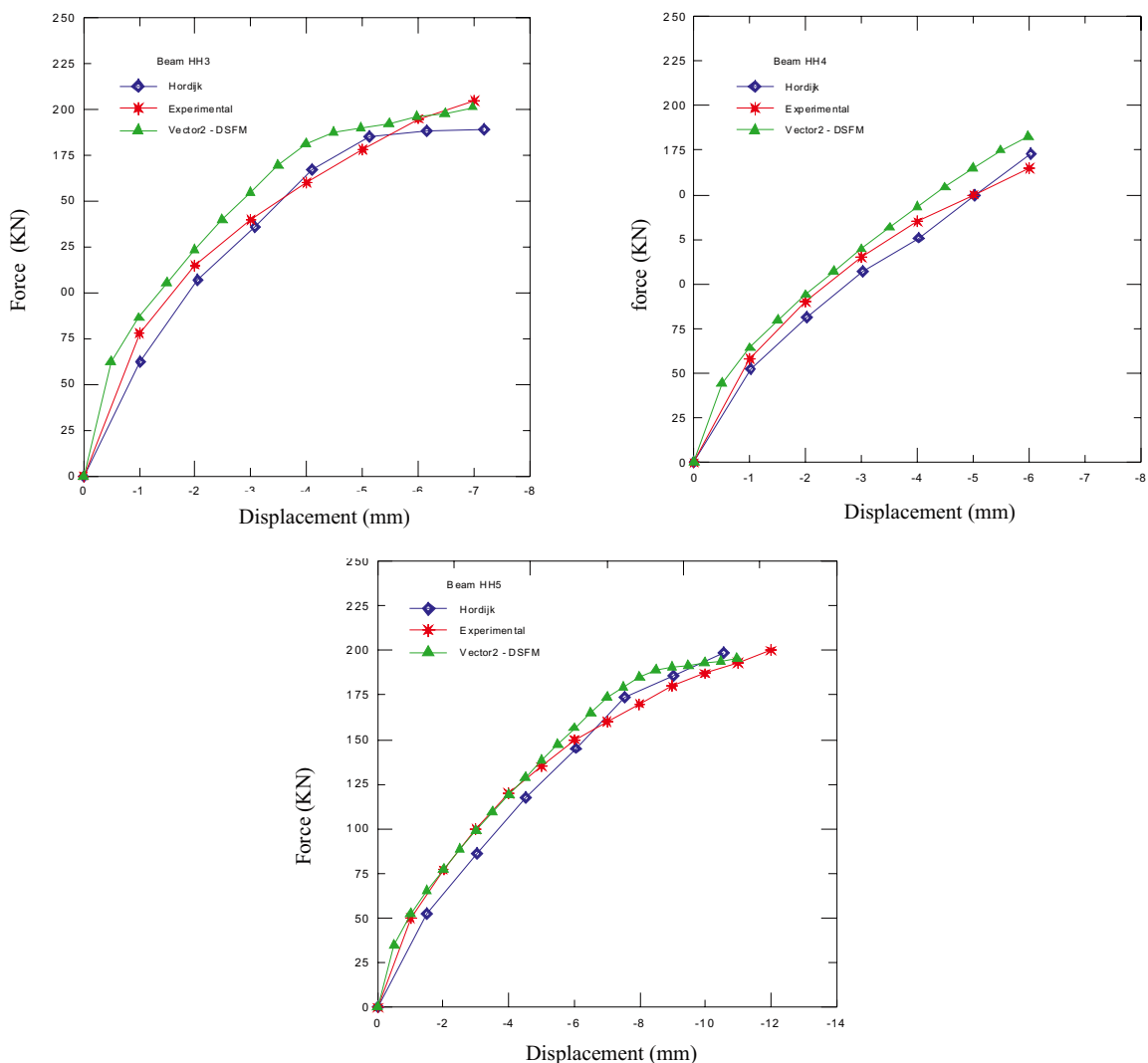
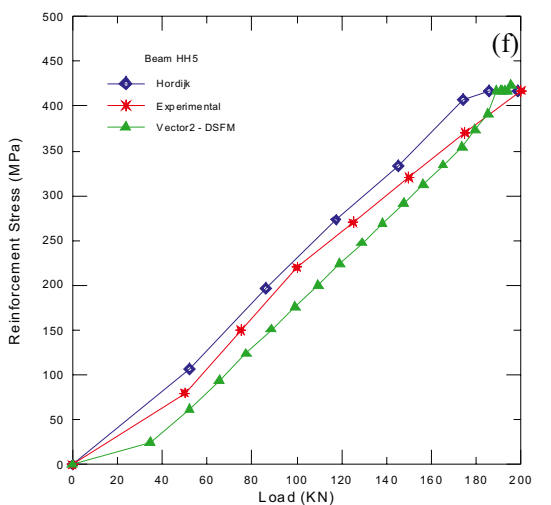
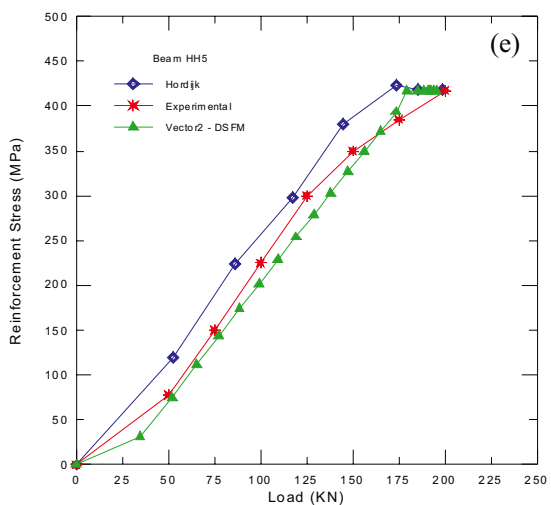
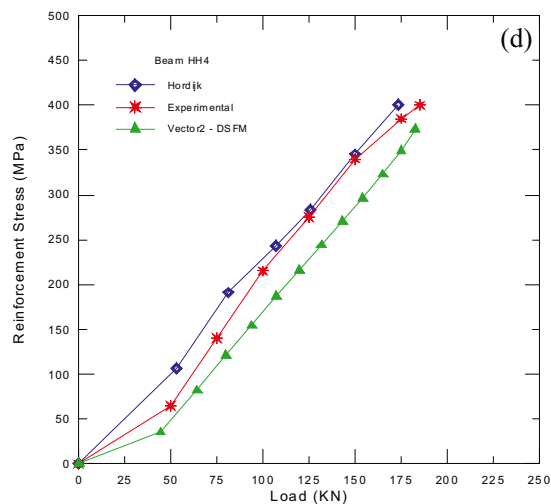
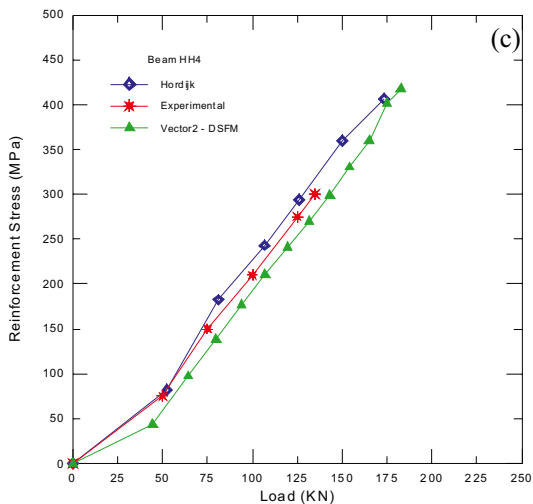
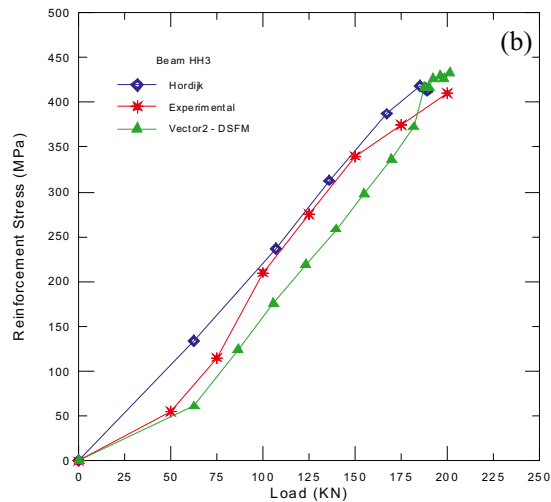
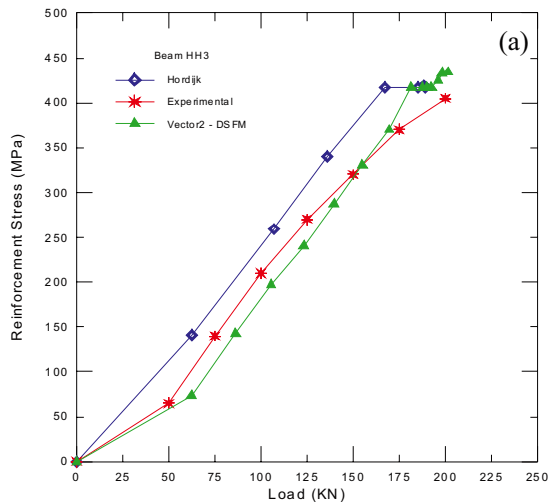


Figure 14 – Reinforcement Stresses (HH3, HH4 and HH5)
(a)negative reinforcement –HH3, (b)positive reinforcement – HH3, (c)negative reinforcement – HH4, (d)positive reinforcement – HH4, (e)negative reinforcement – HH5, (f)positive reinforcement– HH5



- [14] Leonhardt, F. e Walther, R. Beiträge zur Behandlung der Schubprobleme im Stahlbetonbau. Beton-und Stahlbetonbau, v.57, n.7, Berlin, 1962; p.161-173.
- [15] d'Avila, V.M.R. Estudo sobre Modelos de Fissuração de Peças de Concreto Armado via Método dos Elementos Finitos, Porto Alegre, 2003, Tese de

- Doutorado – Universidade Federal do Rio Grande do Sul, 259 p.
- [16] Leonhardt, F. e Walther, R. Beiträge zur Behandlung der Schubprobleme im Stahlbetonbau. Beton-und Stahlbetonbau, v.60, n.2, Berlin, 1965; p.35-42.

Figure 15 – Crack pattern for beam HH5

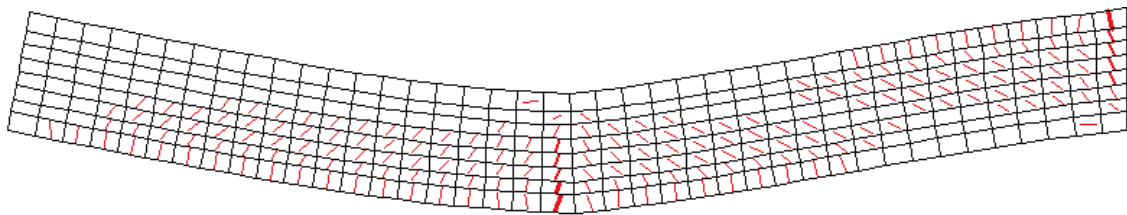
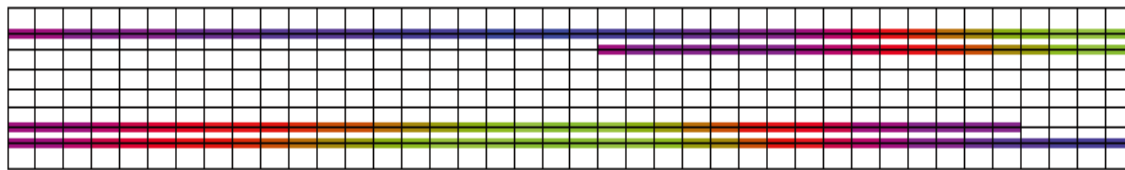


Figure 16 – Reinforcement stresses for beam HH5



HH5		Stress (steel): σ -truss average						Displacement Factor = 11.00			
Blue	to -132.72	Purple	to -36.02	Red	to 60.68	Red	to 157.38	Orange	to 254.08	Light Green	to 350.77
Dark Blue	to -108.55	Dark Purple	to -11.85	Dark Red	to 84.85	Dark Red	to 181.55	Dark Orange	to 278.25	Green	to 374.95
Medium Blue	to -84.37	Medium Purple	to 12.33	Medium Red	to 109.03	Medium Red	to 205.73	Light Green	to 302.43	Light Green	to 399.13
Dark Purple	to -60.20	Dark Purple	to 36.50	Dark Red	to 133.20	Dark Red	to 229.90	Light Green	to 326.60	Light Green	to 423.30